

Study on the tunnel shape and soil-lining interaction influencing the lining behavior under seismic loading

Van Vi Pham^{1†}, Ngoc Anh Do^{1,2‡}, Piotr Osinski^{3‡}, Ngoc Thai Do^{1,2†} and Daniel Dias^{4§}

1. Sustainable Development in Underground Engineering Research Team, Hanoi University of Mining and Geology, Hanoi, Vietnam

2. Department of Underground and Mining Construction, Faculty of Civil Engineering, Hanoi University of Mining and Geology, Hanoi, Vietnam

3. Department of Geotechnical Engineering, Institute of Civil Engineering, Warsaw University of Life Sciences - SGGW, Warszawa, Poland

4. Laboratory 3SR, Grenoble Alpes University, Grenoble 38400, France

Abstract: The response of tunnels subjected to seismic loading is a complex mechanism and depends not only on the seismic nature but also on tunnel structure and surrounding soil properties. The individual behavior of circular, rectangular, and sub-rectangular tunnels subjected to seismic loadings has already been studied in the literature. In the present research, two case scenarios of circular, rectangular tunnels and four sub-rectangular shaped tunnels, with similar cross-section areas, were adopted to perform a comprehensive numerical investigation. The purpose of the study was to determine the mechanical behavior of tunnels of different shapes, depending upon seismic conditions. Analyses were performed by considering the influence of soil-lining interaction, soil parameters, and lining thickness, as well as lining rigidity. Computations were performed for no-slip and full-slip conditions. The results indicate that the tunnel shape design is of great importance when regarding the mechanical behavior of the surrounding soil. This concerns no-slip as well as full-slip soil-lining interaction, especially when the lining is subjected to seismic loading. Moreover, it is shown that changes in incremental bending moments for circular, rectangular and sub-rectangular tunnels that depend upon the soil-lining interaction conditions differ significantly.

Keywords: tunnel shape; soil-lining interaction; seismic loading; internal forces; numerical analysis

1 Introduction

Circular and rectangular shapes are usually chosen for tunnels excavated in urban areas when using mechanized and conventional methods. While a circular tunnel normally provides sufficient tunnel lining stability, rectangular tunnel construction work results in a higher space utilization ratio. To combine the advantages of both tunnel shapes, i.e., sub-rectangular shaped tunnels have recently been developed (Zhang *et al.*, 2017; Liu *et al.*, 2018; Do *et al.*, 2020; Pham *et al.*, 2021, 2023). Studies on tunnel shape that influence lining behavior under static loading conditions have already been performed by several authors (González-Nicieza *et al.*, 2008; Yoon *et al.*, 2014; Vinod and Khabbaz, 2019; Chi

and Alexandr, 2020; Do *et al.*, 2020; Yu *et al.*, 2020; Nguyen *et al.*, 2020). In a number of research studies, it has been established that tunnel linings are subjected to excessive bending moments due to earth pressure and other loadings, resulting in lining cracks and damage, which severely impact a tunnel's stability (Zhang *et al.*, 2019, 2022). These issues are often associated with tunnel shape. Various tunnel geometries are used in tunnel engineering, though circular tunnels are generally preferred due to their ease of construction and function layout. It is important to consider tunnel shape when designing a lining, as an excessive bending moment may arise on the lining under earth pressure if the tunnel shape is unreasonable (Hua *et al.*, 2022).

In recent years, mostly due to demanding global economic growth, underground structures have been widely used to improve transportation conditions, especially in cities, where seismic conditions become a serious safety threat (Choudhury *et al.*, 2019). Most recent state-of-the-art studies clearly show an increased scientific interest in experimental (Abate *et al.*, 2015; Lanzano *et al.*, 2015; Baziar *et al.*, 2016; Wang *et al.*, 2019; Yue and Zheng, 2019; Yang *et al.*, 2022; Cho *et al.*,

Correspondence to: Ngoc Anh Do, Department of Underground and Mining Construction, Faculty of Civil Engineering, Hanoi University of Mining and Geology, Vietnam
Tel.: +84-987.723.686

Email: dongocanh@humg.edu.vn

[†]Doctor; [‡]Associate Professor; [§]Professor

Received May 9, 2023; **Accepted** February 5, 2024

2021; Wu *et al.*, 2024), numerical (Tsinidis *et al.*, 2014; Abate *et al.*, 2015, 2023; Lanzano *et al.*, 2015; Chi and Alexandr, 2020; Wen *et al.*, 2021; Feizi *et al.*, 2022; Shadabi *et al.*, 2022; Lu *et al.*, 2022; Wu *et al.*, 2023; Swati *et al.*, 2024; Pham *et al.*, 2022) and analytical studies (Tsinidis *et al.*, 2020; Liu *et al.*, 2021; Di *et al.*, 2022; Chen *et al.*, 2022, 2023) regarding the design of underground structures when subjected to changing working conditions due to dynamic loading. Such analyses help to gain insight into the seismic behavior and allow for a better understanding of the mechanisms behind the tunneling works and performance in demanding conditions. The literature review shows that over the years particular attention has been paid to the behavior of circular and rectangular tunnels subjected to seismic loading (Wang, 1993; Penzien, 2000; Bobet, 2003; Hashash *et al.*, 2005; Naggar *et al.*, 2008; Kouretzis *et al.*, 2013; Pitilakis *et al.*, 2014; Abate *et al.*, 2015; Baziar *et al.*, 2016; Nguyen *et al.*, 2019; Yue and Zheng, 2019; Sandoval and Bobet, 2020; Sun *et al.*, 2020; Feizi *et al.*, 2022; Wu *et al.*, 2023). Recently, Tsinidis *et al.* (2020) presented a review study of the seismic behavior of tunnels, in which analytical methods, experimental studies, simplified methods, and numerical models for the seismic analysis of circular and rectangular tunnels have been extensively discussed.

Due to the complexity and computational effort required for a full dynamic analysis, simplified analytical or quasi-static numerical calculations are often preferred. Quasi-static numerical analyses allow for an approximation of seismically-induced inertia forces as a constant horizontal acceleration force (Do *et al.*, 2014). In addition to the horizontal acceleration method, Sederat *et al.* (2009) and Do *et al.* (2015) used another quasi-static method, titled ‘ovaling deformations’ in which quasi-static loads are imposed as inverted triangular displacements that are applied along the model’s vertical sides, and constant displacements are imposed along the model’s top. The maximum prescribed displacement assigned to the model’s top is evaluated based on maximum shear strain, γ_{\max} . The work performed by Do *et al.* (2014) indicates that both quasi-static numerical models generate results that are in good agreement with those obtained by Wang’s analytical solution (Wang, 1993).

A review proposed by Fang *et al.* (2023) presents available measures to increase the dynamic strength of tunnels, proving that the properties of the interface surrounding a tunnel lining play a significant role in optimizing tunnel shape and working conditions. The authors indicated that using an imperfect interface causes greater dynamic stress concentration, and a smaller interface stiffness should be introduced to improve tunnel strength. The same conclusion regarding the influence of a soil-lining interface was proposed by Tsinidis *et al.* (2016b), who performed an experimental and numerical investigation for box-type tunnels constructed in dry sand. The bonded soil-lining connection results in a

uniform distribution of soil shear stresses along slabs and side-walls. Full-slip interface conditions lead to shear stress reduction along the middle sections of the slabs and the side-walls, in addition to a remarkable concentration of shear stresses at the corners of the tunnel. Sederat *et al.* (2009) numerically investigated the contact interface effect between the surrounding soil and lining for a circular tunnel subjected to quasi-static loading. The results indicate that the no-slip condition provides the worst state for normal forces in the lining. Similarly, Kouretzis *et al.* (2013) performed a parametric analysis to quantify the influence of interface friction on circular tunnel lining behavior. In contrast to the works of Sederat *et al.* (2009), Kouretzis *et al.* (2013) examined the effect of P-waves as well as S-waves, and the final tunnel lining is assumed not to support any gravity loads that result from soil mass relaxation. Pham *et al.* (2021) investigated a case study in Shanghai, China, by analyzing the behavior of a sub-rectangular tunnel subjected to seismic loading. The results indicated a significant behavior difference between sub-rectangular and circular tunnels. Particular attention was paid to the interaction effect between the tunnel lining and the surrounding soil by considering no-slip and full-slip conditions. Such conditions assume an ideal representation of real contact between the tunnel lining and surrounding material, especially when the structure is subjected to seismic loading (Fang *et al.*, 2023).

The results of the most recent studies indicate that the behavior of sub-rectangular tunnels, when considering soil-lining interface conditions, significantly differs from that of circular-shaped structures. Indeed, while the greater absolute extreme incremental bending moments of a circular tunnel are obtained in the full-slip condition, those of sub-rectangular tunnels in a no-slip condition are greater than the ones in a full-slip condition. This represents an opposite trend to the one observed in circular tunnel linings (Pham *et al.*, 2021).

Tunnel shape causes a significant effect on tunnel lining behavior under seismic loading conditions and should be investigated more fully. The scientific contribution of the present research is that it provides a comprehensive numerical investigation of tunnel shape influence, including circular, rectangular, and sub-rectangular tunnels subjected to seismic loading in both critical soil-lining interfaces of no-slip and full-slip conditions. Such a wide representation of factors that affect the performance of a structure in demanding conditions represents an attempt to further the understanding of dynamic interactions. In the available literature, the studies usually concern analyses of one or two shape types of tunnel construction. However, the present research provides a complete comparison and comprehensive analyses among three different shapes by considering various dimensions of particular cross-sections. This is done to offer a wide picture of soil structure interactions and to describe behavior in different working and design conditions. Two-dimensional

numerical models are adopted to evaluate the influence of the following parameters: seismic acceleration, soil deformation's modulus, tunnel lining thickness, and lining rigidity reduction due to the presence of joints. The variety of parameters considered in the study introduces novelty by broadening our understanding of soil-structure behavior in seismic conditions.

The results indicate a significant impact with regard to tunnel shape and soil-lining interaction. The relationships between the internal forces and the soil Young's modulus, lining thickness, and bending rigidity are different for circular, sub-rectangular, and rectangular tunnels. The results obtained from the study would allow future design optimization for tunnels constructed in ground conditions subjected to seismic loadings.

2 Case study and adopted methodology

The case study concerns an express tunnel located in Shanghai, China. The study assumes six different tunnel cross-section designs, as presented in Fig. 1. Detailed information of dimensions and geometry are listed in Table 1, wherein three major groups of geometry (circular, sub-rectangular and rectangular) were distinguished by considering different configurations of parameters, such as cross-section area, height, width, and radius. The excavation area of all tunnel sections is approximately 59.8 m². For sub-rectangular tunnels, the sections' radii along the tunnel boundary ($R1$, $R3$, and $R2$) refers to the radius of the top and bottom structural elements, side walls, and the shoulder of tunnels, respectively (Fig. 2).

For a better understanding of sub-rectangular tunnel geometry, a detailed cross-section is presented in Fig. 3. For all the cases, the investigated scenarios consider the tunnel to have been excavated at a depth of 10 m in silty clay soil. The geotechnical parameters of the soil profile fed into the model are presented in Table 2. The tunnel is supported by a segmental lining of 0.5 m thickness. To simplify, a continuous lining was assumed, although the joint's effect on lining behavior was not considered, so that the investigated mechanism would be isolated. The tunnel lining parameters are summarized in Table 2, together with soil parameters.

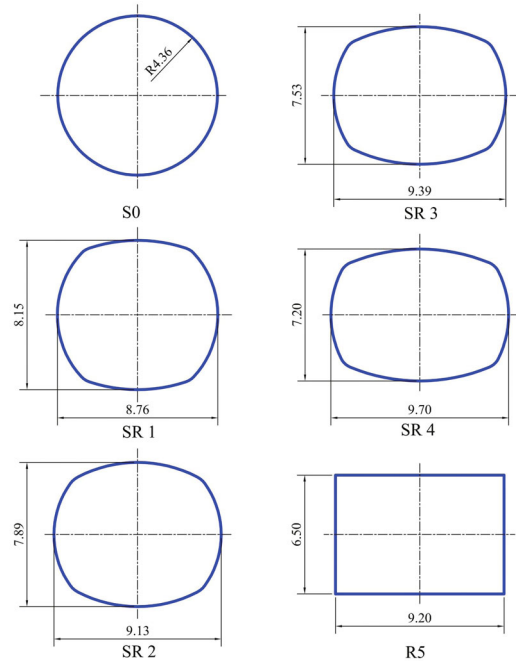


Fig. 1 Cross-sections of the tunnel shapes adopted for the study (dimensions in m)

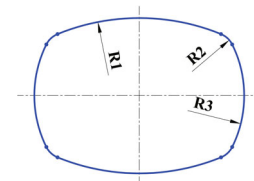


Fig. 2 Definition of the radius for squared and sub-rectangular tunnels

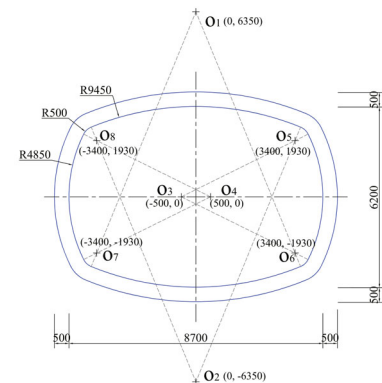


Fig. 3 Sub-rectangular express tunnel dimensions (in mm) (Pham *et al.*, 2022)

Table 1 Geometrical dimensions for tunnel shape case studies

| Case | Tunnel width B (m) | Tunnel height H_t (m) | B/H_t ratio | Radius $R1$ (m) | Radius $R2$ (m) | Radius $R3$ (m) | Tunnel area (m ²) | Type of tunnel shape |
|------|-------------------------|----------------------------|---------------|--------------------|--------------------|--------------------|----------------------------------|-------------------------|
| S0 | 8.72 | 8.72 | 1.000 | 4.36 | - | - | 59.786 | Circular |
| SR1 | 8.76 | 8.15 | 1.075 | 8.36 | 1.02 | 4.99 | 59.788 | Sub-rectangular |
| SR2 | 9.13 | 7.89 | 1.157 | 7.09 | 1.23 | 4.81 | 59.757 | |
| SR3 | 9.39 | 7.53 | 1.247 | 8.50 | 0.96 | 5.07 | 59.778 | |
| SR4 | 9.7 | 7.2 | 1.347 | 9.95 | 1.00 | 5.35 | 59.786 | |
| R5 | 9.2 | 6.5 | 1.415 | - | - | - | 59.800 | Rectangular |

Table 2 Input soil and lining parameters used for the reference case study

| | Parameter | Symbol | Unit | Value |
|--------------------------|--|----------|-------------------|-------|
| Soil properties | Unit weight | γ | kN/m ³ | 18 |
| | Young's modulus | E | MPa | 100 |
| | Poisson's ratio | ν | - | 0.34 |
| | Internal friction angle | ϕ | degrees | 33 |
| | Cohesion | C_u | kPa | 0 |
| | Lateral earth pressure coefficient | K_0 | - | 0.5 |
| | Depth of tunnel | H | m | 20 |
| Tunnel lining properties | Peak horizontal acceleration at the ground surface | a_H | g | 0.5 |
| | Young's modulus | E_l | GPa | 35 |
| | Poisson's ratio | ν_l | - | 0.15 |
| | Lining thickness | t | m | 0.5 |
| | External diameter | D | m | 9.76 |

3 Numerical model

First, a numerical model for the circular tunnel was developed by using finite difference method-based software (FLAC^{3D}) (Itasca, 2016). A 2D plane strain model, in quasi-static loading conditions, was generated, and is presented in Fig. 4. The soil model is discretized into hexahedral zones. The tunnel lining is modeled by embedded liner elements, which are attached to the soil zones through interfaces. The normal stiffness, k_n , and tangential stiffness, k_s , of the liner zone interface are determined based on recommendations given in (Itasca, 2016), where k_n and k_s are set equal to 100 times the equivalent stiffness of the stiffest neighboring zone. This is done to keep the interface deformation small and relative to the analyzed zone. Two critical conditions of no-slip and full-slip at the ground-support interface were considered by changing interface cohesion. When the no-slip condition is applied, the cohesion is assigned to be very high to ensure that there is no relative shear displacement along the ground-support interface. Meanwhile, no shear stress transmission along the interface is assumed by adopting a zero cohesion value in the case of the full-slip condition (Itasca, 2016), due to the smooth contact surface conditions applied in the analyses.

The mesh is composed of a single layer of y-direction zones, in which the dimension of the elements increases with distance from the tunnel. Dimensions of the numerical model are 120 m in the x-direction and 40 m

in the z-direction. The model consists of approximately 4800 zones and 9800 nodes. The model bottom was restrained in all directions, while the vertical sides were fixed horizontally since the small strain mode was adopted for computations. The soil and tunnel lining were assumed to be linear-elastic material, such as those adopted in the analytical solution proposed by Wang (1993).

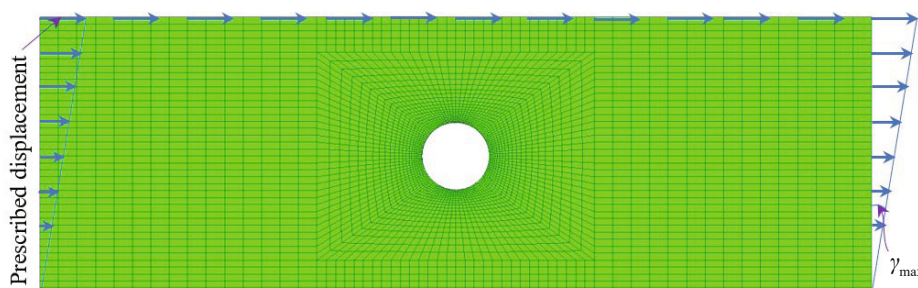
In the present study, the ovaling deformations caused by seismic loading are assigned as inverted triangular displacements along the vertical sides. Constant horizontal displacements are assigned along the surface of the model (Pham *et al.*, 2021). The prescribed displacements applied at the surface are determined, based on maximum shear strain γ_{\max} .

The shear strain γ_{\max} can be determined as follows (Newmark, 1967; Hashash *et al.*, 2001; FHWA, 2004):

$$\gamma_{\max} = \frac{V_{\max}}{V_s} \quad (1)$$

where V_{\max} is the peak shear wave velocity and V_s is the ground shear wave velocity. V_{\max} depends upon the known peak ground acceleration a_H and the depth of the tunnel.

Before assigning the ovaling deformations caused by seismic loading, the tunnel was considered to be in a steady state, and was excavated under static conditions. The procedure for the tunnel ovaling numerical simulation was therefore conducted as follows:

**Fig. 4** Numerical model of the circular tunnel in quasi-static loading conditions

- Step 1: Establishing the in-situ equilibrium state of the model before tunnel construction;
- Step 2: Excavation of the tunnel under static conditions. The concrete lining is then activated on the tunnel boundary;
- Step 3: Assigning the prescribed ovaling displacements caused by seismic loading on the two vertical sides and at the top of the model. The prescribed displacement applied at the model's top is evaluated by multiplying the shear strain value and the model's height.

It should be noted that only the incremental internal forces, i.e., bending moment and normal forces, as caused by the seismic loading are presented in the study. They are calculated by subtracting the total lining forces computed at the static loading stage end (step 2) from those determined at the ovaling ending stage (step 3).

Results obtained from the numerical computations for the case of a circular tunnel under quasi-static

loading and in both no-slip and full-slip conditions were validated by comparison with the commonly known analytical method proposed by Wang (1993), using the input data described in Table 2 (Pham *et al.*, 2021). Based on the validated model of the circular tunnel, other numerical models of sub-rectangular and rectangular tunnels were developed. Figure 5 presents an example of the SR4 tunnel shape case, applying the same boundary conditions under static and quasi-static loadings.

4 Influence of tunnel shape on the lining behavior

Figure 6 presents the incremental internal forces distribution along the tunnel lining with the extreme values, i.e., maximum and minimum, as given and displayed in Table 3. Parameters of the soil, tunnel lining, and earthquake acceleration that were introduced

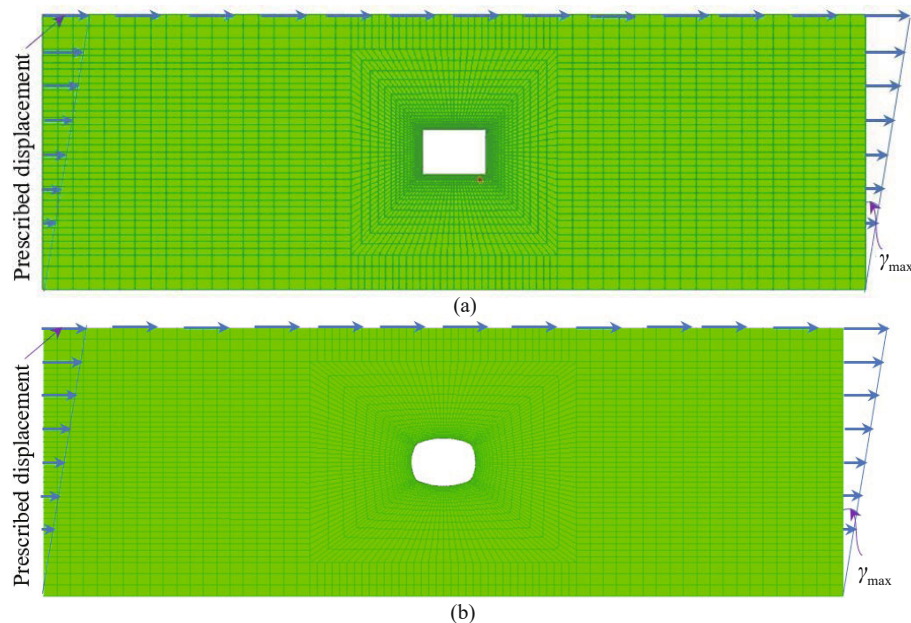


Fig. 5 Numerical model in quasi-static loading conditions of: (a) a rectangular tunnel and (b) a sub-rectangular tunnel, shape case SR4

Table 3 Incremental forces induced in different tunnel linings

| No. | Tunnel shape | Soil-lining interaction | M_{\max} (MN·m/m) | M_{\min} (MN·m/m) | N_{\max} (MN/m) | N_{\min} (MN/m) | T_{\max} (MN/m) | T_{\min} (MN/m) |
|-----|--------------|-------------------------|------------------------|------------------------|----------------------|----------------------|----------------------|----------------------|
| 1 | R0 | No-slip | 0.753 | -0.755 | 0.832 | -0.823 | 0.344 | -0.349 |
| | | Full-slip | 0.843 | -0.844 | 0.190 | -0.196 | 0.383 | -0.393 |
| 2 | SR1 | No-slip | 0.842 | -0.843 | 0.791 | -0.789 | 0.319 | -0.320 |
| | | Full-slip | 0.869 | -0.863 | 0.173 | -0.169 | 0.363 | -0.299 |
| 3 | SR2 | No-slip | 0.848 | -0.849 | 0.798 | -0.797 | 0.345 | -0.256 |
| | | Full-slip | 0.842 | -0.815 | 0.179 | -0.171 | 0.402 | -0.251 |
| 4 | SR3 | No-slip | 0.875 | -0.878 | 0.796 | -0.790 | 0.354 | -0.252 |
| | | Full-slip | 0.830 | -0.783 | 0.168 | -0.170 | 0.407 | -0.259 |
| 5 | SR4 | No-slip | 0.899 | -0.900 | 0.791 | -0.794 | 0.367 | -0.270 |
| | | Full-slip | 0.807 | -0.762 | 0.159 | -0.153 | 0.419 | -0.264 |
| 6 | R5 | No-slip | 1.103 | -1.108 | 0.561 | -0.559 | 0.746 | -0.625 |
| | | Full-slip | 0.845 | -0.768 | 0.111 | 0.013 | 0.309 | -0.301 |

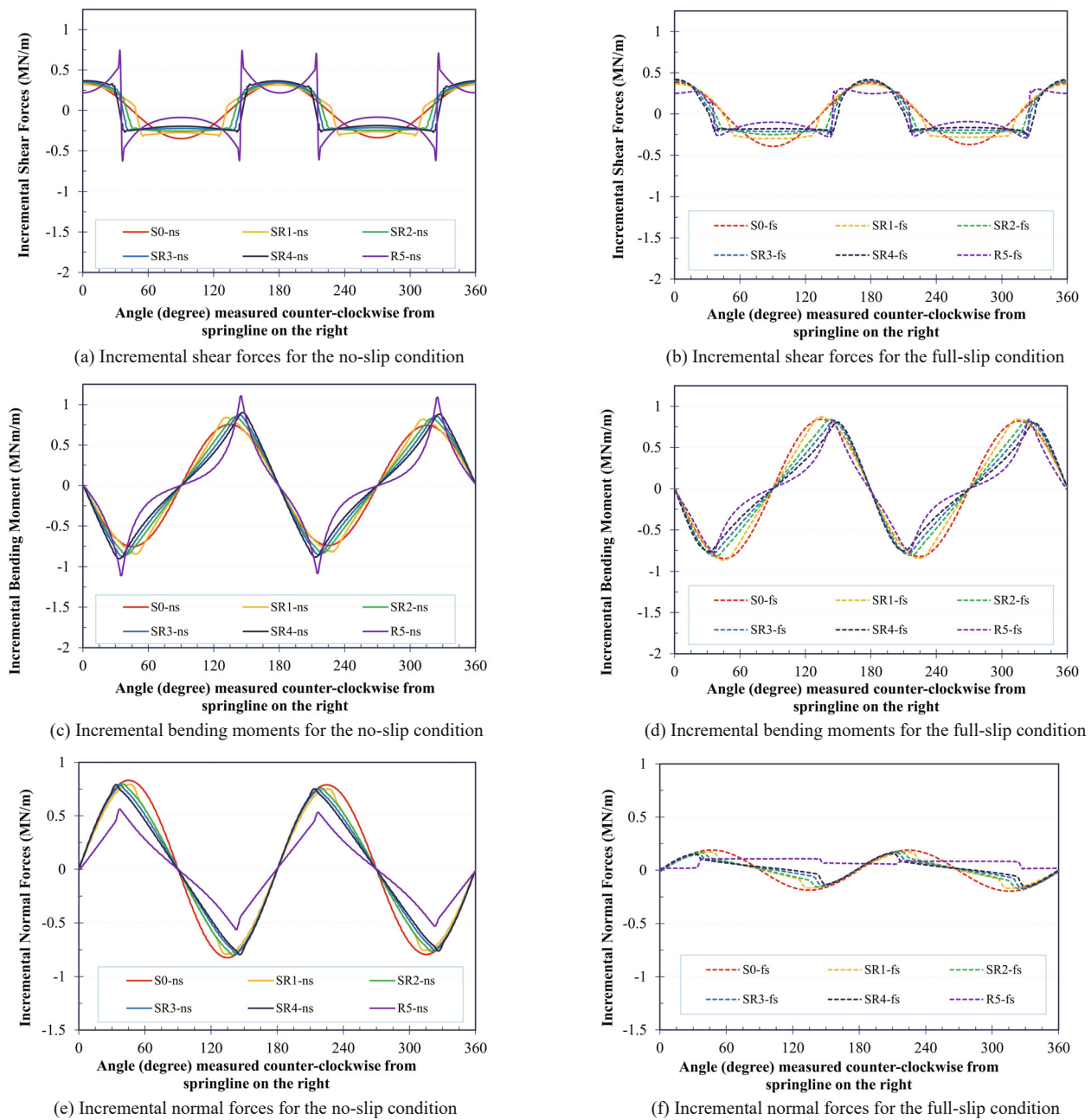


Fig. 6 Distribution of the incremental internal forces in analyzed tunnels

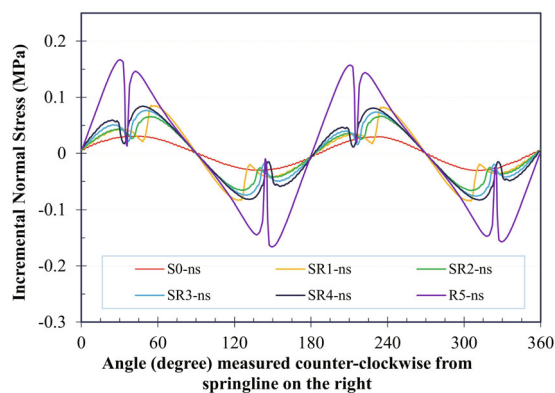
in Table 2 are adopted. The results indicate the significant influence of tunnel shape on the behavior of lining under seismic conditions as well as soil-lining interaction.

Figures 6(a) and 6(b) illustrate the extreme incremental shear forces in the tunnel lining. The results showed that the extreme incremental shear forces in sub-rectangular tunnels are usually induced at the corners with the smallest periphery radius. The absolute extreme incremental shear forces in the sub-rectangular tunnels increased slightly when the tunnel shapes changed from SR1 to SR4 (Table 3). The largest shear force is observed at the rectangular tunnel corners for the no-slip condition. It is approximately two times larger than the ones observed in the sub-rectangular and circular tunnels,

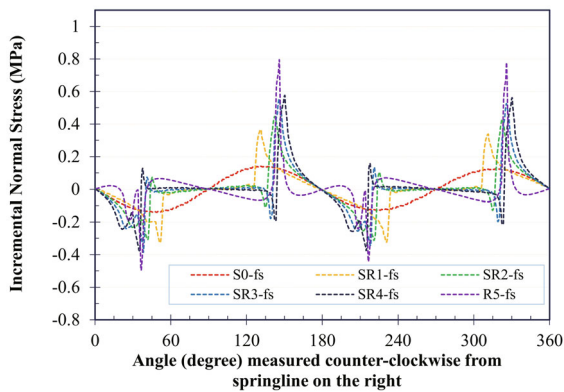
while the absolute extreme incremental shear forces noted in the rectangular tunnel case SR1 are the smallest. Except for the rectangular tunnel case, the maximum incremental shear forces induced in the circular and sub-rectangular tunnels for the no-slip condition are always smaller than the ones for the full-slip condition. These results indicate that the tunnel shapes and the soil-lining interaction have a significant effect on the shear forces distribution induced in the tunnel lining.

Figures 6(c) and 6(d) indicate that the extreme incremental bending moments in the sub-rectangular tunnels are usually induced at corners that are assigned with the smallest tunnel periphery radius. However, the absolute extreme incremental bending moments in

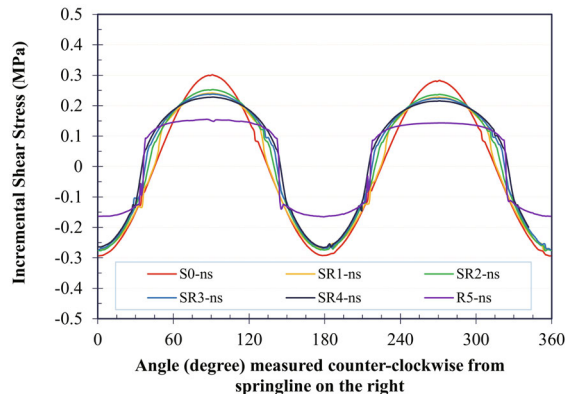
the sub-rectangular tunnels are nearly the same (10% larger than for the circular tunnel analyses). The biggest bending moment is observed at the rectangular tunnel corners. It is worth emphasizing that there are inflection points on the bending moment diagrams along the tunnel boundary. At these points the bending moments change from positive to negative values. These points are located at the top and bottom midpoint parts, as well as on the side walls, which correspond to the transition position between compressive and tension contact stresses in the tunnel lining. It should be mentioned that the positive and negative values illustrated in Figs. 7(a) and 7(b) correspond to the compressive and tension normal contact stresses, respectively.



(a) Incremental normal pressures for no-slip conditions



(b) Incremental normal pressures for full-slip conditions



(c) Incremental tangential pressures for no-slip conditions

Fig. 7 Distribution of the incremental contact stresses in the analyzed tunnels

Results presented in Table 3 indicate that the absolute extreme incremental bending moment of the circular tunnel in the full-slip condition is 12% greater than those corresponding to the no-slip condition. This finding is consistent with the one obtained by a closed-form solution (Wang, 1993) and the literature available on numerical analysis (Sederat *et al.*, 2009; Do *et al.*, 2015; Fang *et al.*, 2023). However, when the tunnel shape changes to a sub-rectangular form, the influence of soil-lining interaction on the absolute extreme incremental bending moment depends upon the ratio between the width (B) and the height (H_t) of the tunnel. In tunnel shape case SR1, in which the B/H_t ratio is close to 1, the absolute extreme incremental bending moment for the no-slip and full-slip conditions are nearly the same. However, when the B/H_t ratio increases, i.e., for sub-rectangular cases SR2, SR3, and SR4, the absolute extreme incremental bending moment for the no-slip condition tends to increase. Its value for the full-slip condition is reduced and even smaller than for the no-slip condition. In rectangular tunnel case (R5), the absolute extreme incremental bending moment for the no-slip condition is 30.5% larger than for the full-slip condition.

Figures 6(e) and 6(f), and Table 3 show significant differences between the incremental normal forces induced along the tunnel lining in two critical conditions of no-slip and full-slip analyses. Therefore, the soil-lining interface imposes a stronger effect on the incremental normal forces of the tunnel lining. In contrast to the bending moments, the absolute extreme incremental normal forces induced in the no-slip analysis are always greater than those for the full-slip condition. The same finding is presented by Tsinidis *et al.* (2016a, 2016b), in which the authors indicate that dynamic axial force increments for full-slip are much lower than in the case of no-slip analysis.

The greatest incremental normal force is obtained for circular tunnels, while a rectangular tunnel induces the smallest incremental normal force. The values for sub-rectangular tunnels fall in a range in between. It is important to note that the B/H_t ratio change of the sub-rectangular tunnels causes an insignificant variation of the absolute extreme incremental normal forces. It should be noted that for the full-slip analysis, the normal force increases exclusively due to the soil's normal contact pressure. However, in the no-slip analysis case, the normal forces increment is developed due to the normal and tangential tension at the soil-lining interface. The higher incremental normal forces in the no-slip analysis could be explained by the fact that the soil-lining interface is locked in a tangential direction. This allows for a considerable buildup of normal forces (Sederat *et al.*, 2009; Fang *et al.*, 2023). The smaller normal forces increment in the rectangular tunnel case can be explained by the inability of normal forces to be transferred from the side walls to the top and bottom parts, and vice versa. On the other hand, in the case of circular and sub-rectangular tunnels, normal forces can

be transferred between the tunnel lining elements due to the continuously curved shapes, especially at the corners of the sub-rectangular tunnel.

Figure 6(f) also indicates an interesting phenomenon whereby incremental normal forces induced in the rectangular tunnel during full-slip analysis are nearly always greater than zero. This implies that there is no normal tension force developed in the rectangular tunnel lining under seismic loading. First, This could be explained by the absence of shear contact stress applied along the straight sections of the rectangular tunnel lining's external boundary in full-slip analysis. This provides the reason for the lack of incremental tangential pressures for the full-slip conditions shown in Fig. 7. Furthermore, the maximum incremental compressive normal contact stresses induced at the top-left and bottom-right corners of the rectangular tunnel lining are significantly greater than the absolute values of the minimum stresses induced at the two other corners, as presented in Fig. 7(b). It is therefore the incremental compressive force that is predominantly applied in a rectangular tunnel lining. It also is important to note that the distribution of normal forces along the tunnel lining depends upon the lining's slenderness ratio and rigidity. Greater lining rigidity will allow a higher transmission ability for normal forces. On the other hand, tensile normal forces can be observed in flexible linings. It is worth noticing that shear stresses are induced in the soil surrounding the tunnel. They increase at the tunnel's corners (Tsinidis *et al.*, 2016a, 2016b) and do not cause a significant effect on the incremental lining normal forces, as long as the full-slip condition is taken into consideration. The reason for this is that in the present study the lining surface is assumed to be smooth, whereas the research conducted by Tsinidis *et al.* (2016a, 2016b) was performed for rough surfaces while considering the friction influence along the lining.

Figures 7(a) and 7(b) indicate that incremental normal contact stresses distributed along the tunnel lining are highest in the rectangular tunnel and smallest in the circular one. The largest values are always seen at the positions close to the corners of the rectangular

and sub-rectangular tunnels, while at these positions the incremental tangential contact stresses (see Fig. 7(c)) are nearly zero. The extreme incremental tangential contact stresses are obtained at the middle points of the top, bottom, and side walls of the tunnels.

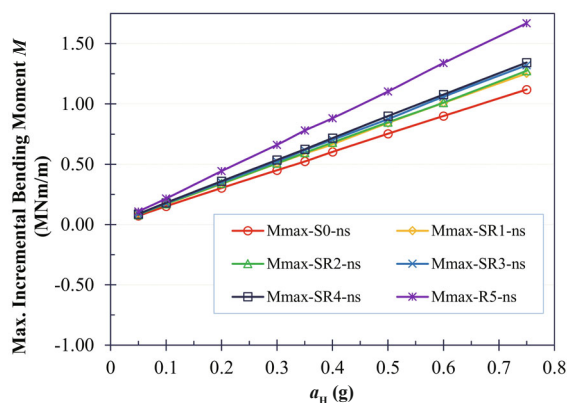
5 Parametric analysis

5.1 Influence of maximum horizontal acceleration (a_H)

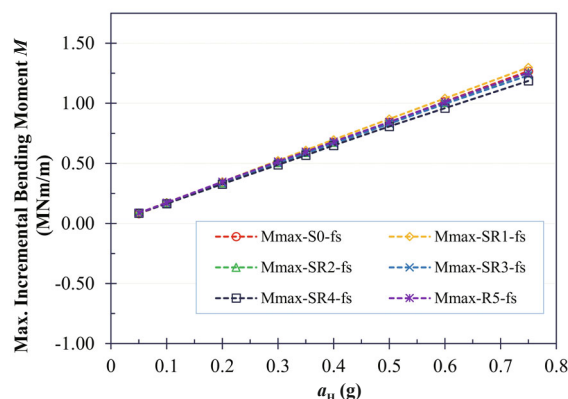
A parametric analysis is conducted to highlight the impact of the maximum horizontal acceleration (a_H), the soil Young's modulus (E), the lining thickness (t), and the reduction factor of tunnel lining rigidity (η) on the incremental internal forces induced in the tunnel lining when considering the six tunnel shapes and the lining-soil interaction.

The maximum horizontal acceleration, a_H , is assumed to change in a range from 0.05 to 0.75 g, corresponding to shear strains (γ_c) falling in the range between 0.038% and 0.57%. Other parameters of the reference case study are adopted as listed in Tables 1 and 2. High horizontal accelerations (a_H), imply high shear strains (γ_{max}); therefore, this results in high absolute extreme incremental bending moments and normal forces. The linear relationship is presented in Figs. 8 and 9.

Figures 8(a) and 8(c) indicate that the maximum horizontal acceleration influence on the extreme incremental bending moments, induced in circular and rectangular tunnels, is different from sub-rectangular tunnel cases for the no-slip analysis. The rectangular tunnel is the most sensitive shape, and the circular tunnel is less influenced by the a_H values change. The results are obtained for a sub-rectangular fall in between those two cases. The higher the maximum horizontal acceleration, the greater the tunnel shape's influence on the incremental bending moment. Special attention should be paid to the relatively similar bending moments in sub-rectangular tunnels. This could be related to the small radius $R2$ difference at the corners of the sub-rectangular tunnel, as indicated in Table 1. Unlike

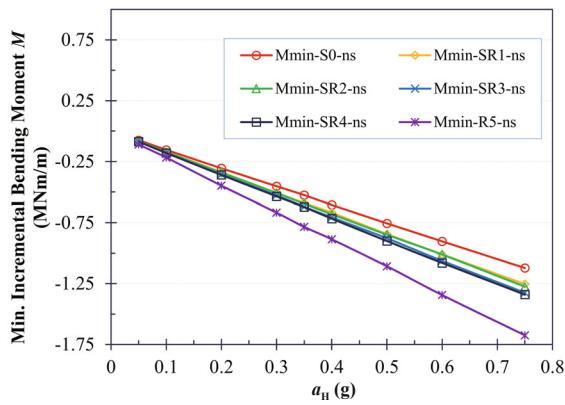


(a) Max. incremental bending moment in the no-slip condition

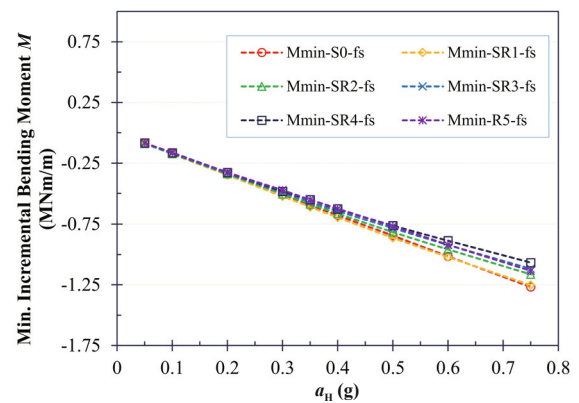


(b) Max. incremental bending moment in the full-slip

Fig. 8 Effect of a_H on the extreme incremental bending moments of tunnel linings

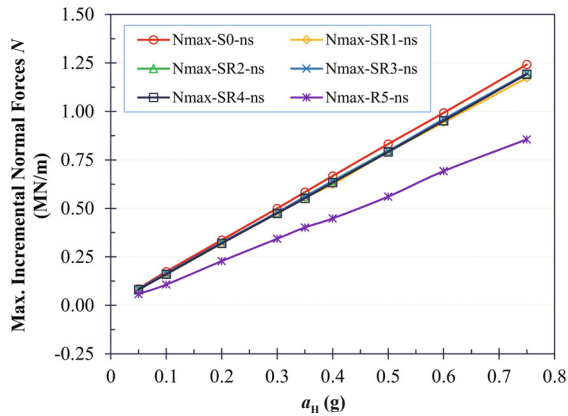


(c) Min. incremental bending moments for no-slip conditions

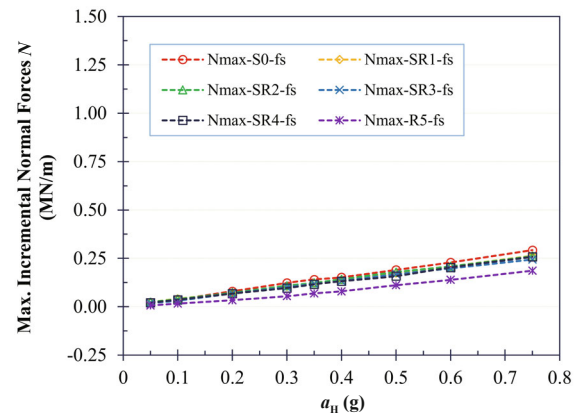


(d) Min. incremental bending moments for full-slip conditions

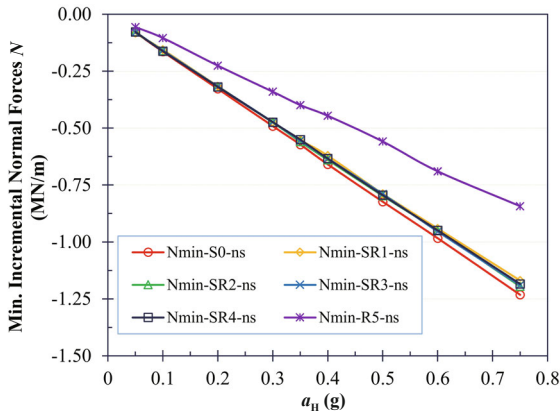
Fig. 8 Continued



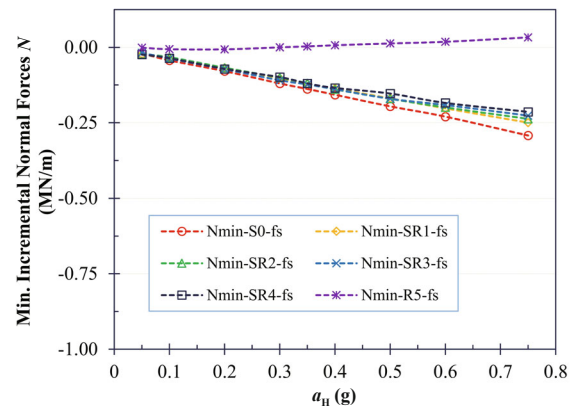
(a) Max. incremental normal forces for no-slip conditions



(b) Max. incremental normal forces for full-slip conditions



(c) Min. incremental normal forces for no-slip conditions



(d) Min. incremental normal forces for full-slip conditions

Fig. 9 Effect of a_H on the extreme incremental normal forces of tunnel linings

the no-slip analysis, Figs. 8(b) and 8(d) show a very small tunnel shape influence on the extreme incremental bending moments under seismic loading, especially for low maximum horizontal accelerations. In addition, the results also indicate that when maximum horizontal acceleration is greater, the soil-lining interaction effect, i.e., no-slip and full-slip conditions on the extreme incremental bending moment, also increases.

Figures 9(a) and 9(c), show an increase of the extreme incremental normal forces in the tunnel lining when the maximum horizontal acceleration reaches higher values.

The absolute extreme incremental normal forces in the rectangular tunnel are always the smallest, while for sub-rectangular tunnels they are similar, although slightly lower than for circular tunnel geometries. In addition, rectangular tunnels are less sensitive to the maximum horizontal acceleration change than other tunnel shapes. The small maximum horizontal acceleration effect on the incremental normal forces in the full-slip analysis could be referred to as the lack of tangential tension at the soil-lining interface. Figure 9(d) also indicates that incremental normal forces, induced in the rectangular

tunnel during full-slip analysis, are typically greater than zero, which implies the impact of compressive incremental normal forces in the tunnel lining.

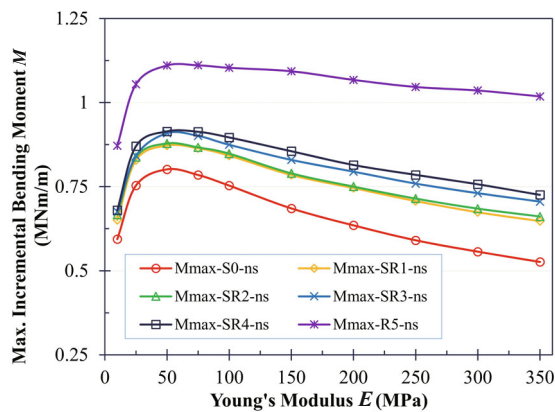
5.2 Influence of the soil Young's modulus (E)

Soil Young's modulus has been considered to vary in a range from 10 MPa to 350 MPa, which corresponds to the case of soft soils to soft rocks. The reference parameters are listed in Tables 1 and 2. For all the considered tunnel shapes and in both soil-lining interactions, i.e., no-slip and full-slip, for small soil Young's modulus (E), an increase of the E value causes greater absolute extreme incremental bending moments, as presented in Fig. 10. The peaks of the extreme incremental bending moments are generally reached for a soil Young's modulus of approximately 50 MPa. When the soil Young's modulus continues to increase, a gradual reduction of the absolute extreme incremental bending moments is observed. Only a small correlation exists when the function drops down. This could be explained by the fact that when the ground is softer than the tunnel lining, the lining tends to resist the ground displacements, and therefore an increase of incremental bending moment is expected. On the other hand, when the lining is more flexible than the surrounding ground, the lining will experience amplified distortions when compared to the ground shear distortions in the free space. Hence, a gradual decrease in the incremental bending moments can be predicted

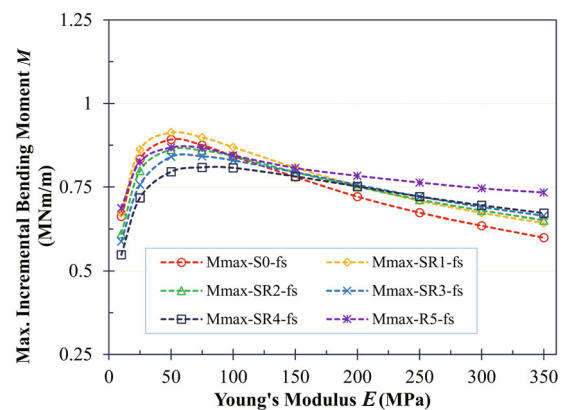
(Pham *et al.*, 2021). This extreme incremental bending moment variation tendency, depending on the soil Young's modulus of the soil, is different from the lining bending moments under static loading. This conclusion complies with the findings published by Do *et al.* (2020), in which a decrease in the bending moments along with an increase in the soil Young's modulus was presented.

It should be also noted that for the same soil Young's modulus value, the absolute extreme incremental bending moments induced in the rectangular tunnels are greater than the sub-rectangular and circular ones for a no-slip analysis (Figs. 10(a) and 10(c)). The smallest values are obtained for the circular ones. Nevertheless, for the full-slip analysis (Figs. 10(b) and 10(d)), when the soil Young's modulus is smaller than 150 MPa, the greatest maximum incremental bending moments are observed in the sub-rectangular tunnels (case SR1), followed by the circular tunnel case. For greater soil Young's moduli, maximum incremental bending moments are observed for the rectangular tunnel case, whereas the smallest moments are induced for the circular tunnel.

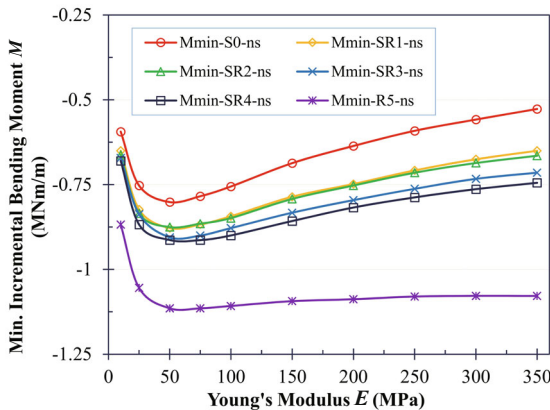
Figures 11(a) and 11(c) show a rapid increase for the absolute extreme incremental normal forces in the tunnel lining for the no-slip analysis when the E value increases. Figures 11(a) and 11(c) allow for identifying the smallest absolute extreme incremental normal forces in the rectangular tunnel; for the circular tunnel, the effect is the opposite. The values for sub-rectangular



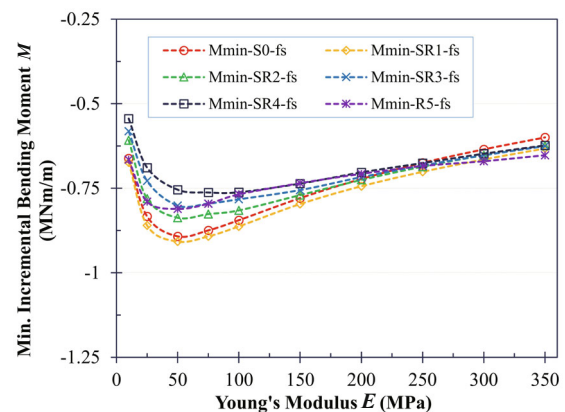
(a) Max. incremental bending moments for the no-slip condition



(b) Max. incremental bending moments for the full-slip condition



(c) Min. incremental bending moments for the no-slip condition



(d) Min. incremental bending moments for the full-slip condition

Fig. 10 Effect of E on the incremental bending moments of tunnel linings

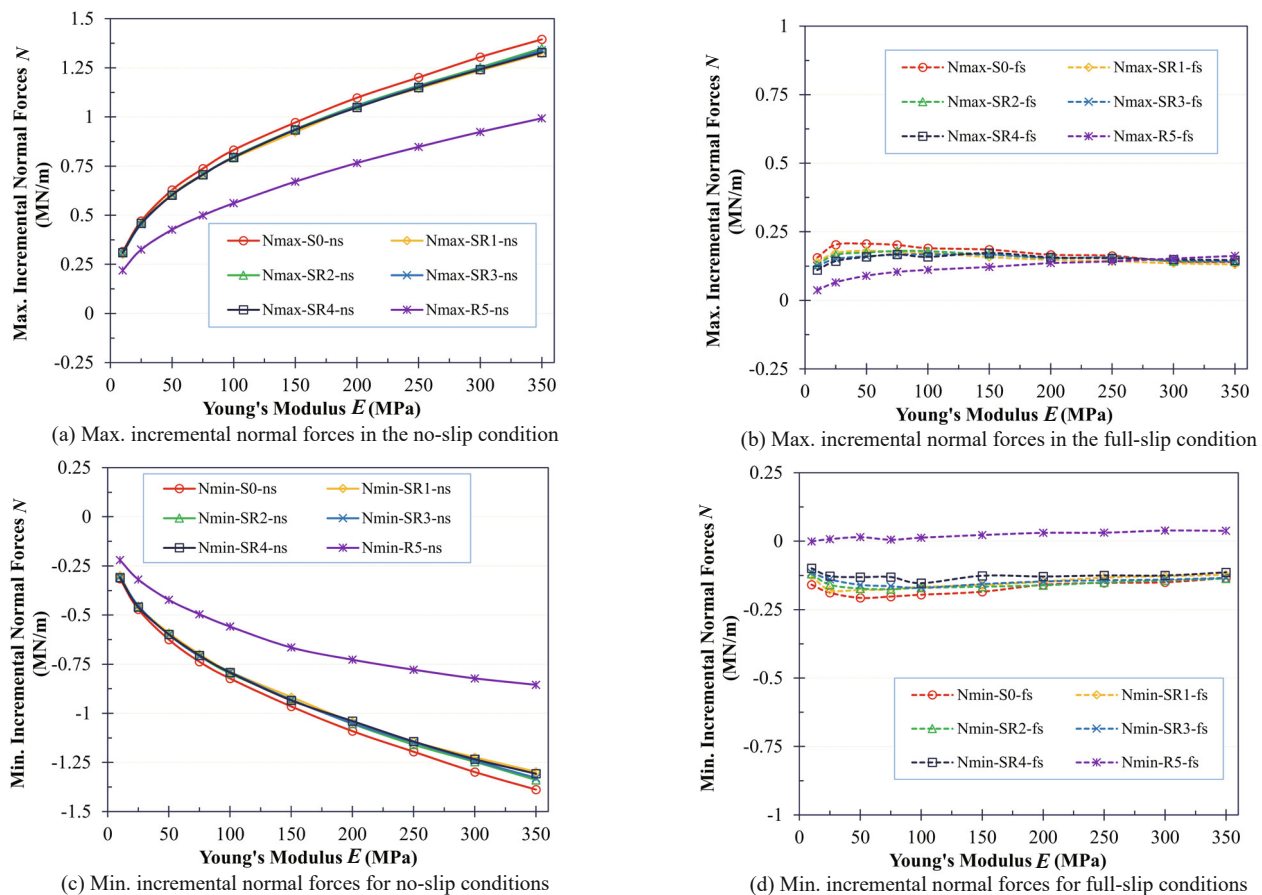


Fig. 11 Effect of E on the incremental normal forces of the tunnel linings

tunnels fall in the range between those two. As for the maximum horizontal acceleration effect, the absolute extreme incremental normal forces in all sub-rectangular tunnels are similar to all investigated values of soil Young's modulus.

Unlike the no-slip analysis, Figs. 11(b) and 11(d) present an insignificant influence of the soil Young's modulus on the extreme incremental normal forces for the full-slip analysis, especially in the rectangular tunnel case. The reason for this could be explained by the lack of tangential tension along the tunnel periphery.

Figure 11(d) also indicates the impact of compressive incremental normal forces in the rectangular tunnel lining.

The following section illustrates the effects of the tunnel shape and soil-lining condition on the tunnel lining displacements, presented through the Δ_{str}/Δ_{fr} ratio when considering the change in the soil Young's modulus (E). This relationship is presented in Fig. 12. Also, Δ_{str} and Δ_{fr} imply the maximum displacement of the lining and the soil in a free zone, without structure, at the corresponding position, and under seismic loadings. The Δ_{str}/Δ_{fr} ratio implies that when its value is smaller

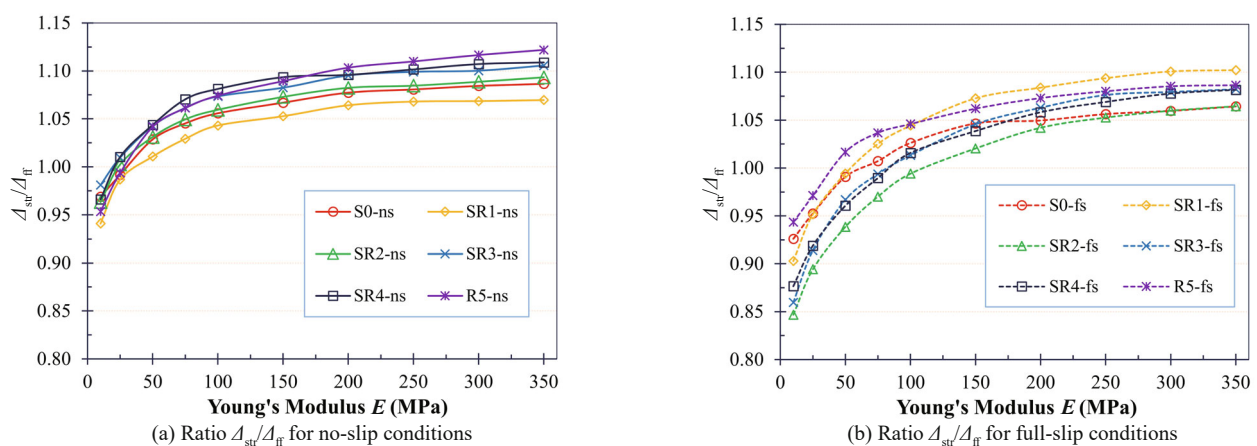


Fig. 12 Effect of E on the relative displacement's ratio considering different shaped tunnels

than unity, the lining is stiffer than the surrounding soil and it tends to resist soil displacements. On the other hand, when the ratio of Δ_{str}/Δ_{ff} is greater than unity, then the lining is more flexible than the soil. Therefore, the lining will experience amplified distortions compared to the ground shear distortions in the free zone. The same finding was indicated by Sandoval Bobet (2020), and Golshani and Rezaeibadashiani (2020). It is reasonable to conclude that the Δ_{str}/Δ_{ff} ratio increases with higher soil Young's moduli. This finding is observed in both no-slip and full-slip soil-lining conditions. In addition, the ratio Δ_{str}/Δ_{ff} in the no-slip analysis is usually greater than for the full-slip condition.

Figure 12 shows a greater effect of Young's modulus (E) on the Δ_{str}/Δ_{ff} ratio when E values are smaller than 100 MPa. When E values exceed 100 MPa, this results in an insignificant change in the ratio (Δ_{str}/Δ_{ff}). In the no-slip condition, when Δ_{str}/Δ_{ff} is smaller than unity, the critical E value is smaller than the one of the corresponding tunnel in the full-slip analysis.

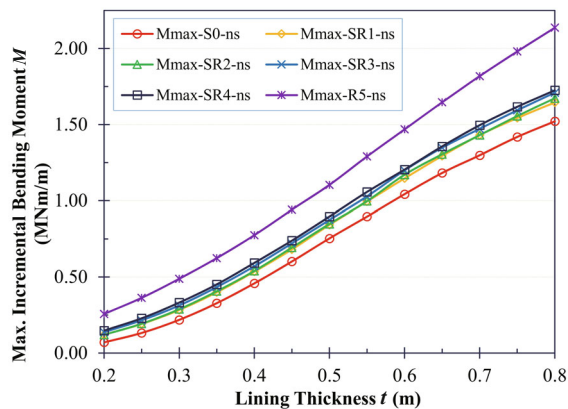
5.3 Influence of the lining thickness (t)

The present analyses assume a lining thickness in the range of 0.2–0.8 m. Figure 13 proves that the extreme incremental bending moments linearly increase with the lining thickness for both the no-slip and full-slip analyses. In the no-slip analysis, relationship lines are

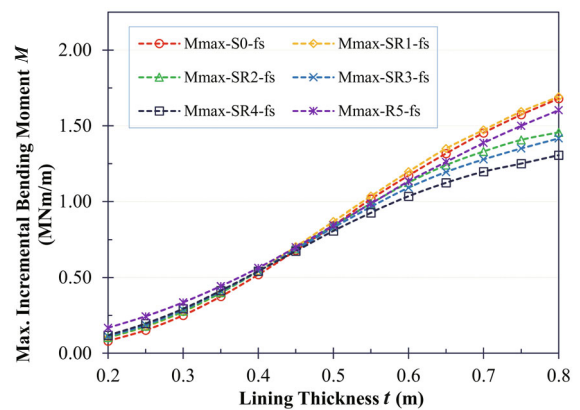
almost parallel. The rectangular shape tunnel gives the highest values, whereas the circular one provides the smallest. The results for sub-rectangular tunnels fall in the range in between them. The full presentation of results is given in Figs. 13(a) and 13(c). In the full-slip analysis, the extreme incremental bending moments slightly change when the lining thickness is lower than 0.5 m (Figs. 13(b) and 13(d)). The smallest values were obtained for circular tunnels. For thicker linings, the circular and sub-rectangular SR1 tunnels cause the greatest absolute extreme incremental bending moments, and the sub-rectangular tunnel SR4 gives the smallest values. It should be noted that the tunnel height/width ratio in the sub-rectangular tunnel SR1 is close to 1.

As presented in Figs. 14(a) and 14(c), similar to the effect of the maximum horizontal accelerations and soil Young's moduli, the absolute extreme incremental normal forces in all sub-rectangular tunnels are similar for all the investigated lining thicknesses in the no-slip analysis. The values are smaller than for circular tunnels but significantly larger than for rectangular tunnels.

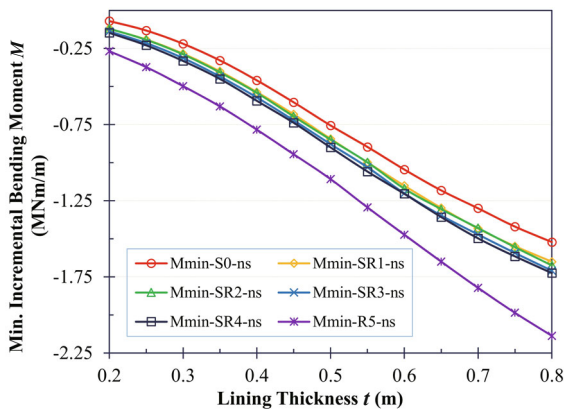
In the full-slip analysis, larger lining thicknesses cause an increased impact of the tunnel shape on the extreme incremental normal forces, as seen in Figs. 14(b) and 14(d). It is worth noting that for the largest lining thickness, the largest and smallest absolute extreme incremental normal forces are observed in circular and rectangular tunnels. For tunnel cases from SR1 to



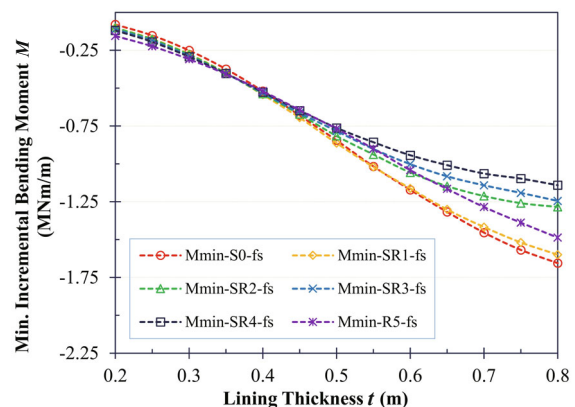
(a) Max. incremental bending moments for no-slip conditions



(b) Max. incremental bending moments for full-slip conditions

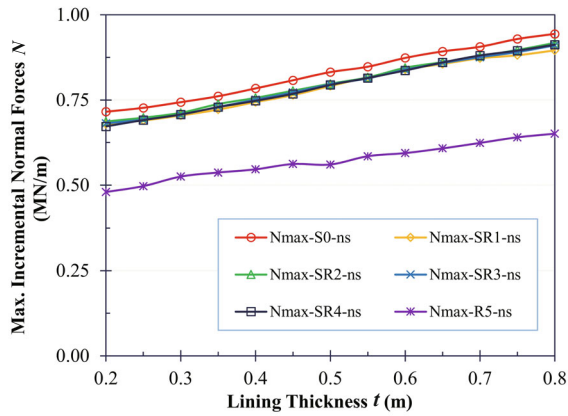


(c) Min. incremental bending moment for no-slip conditions

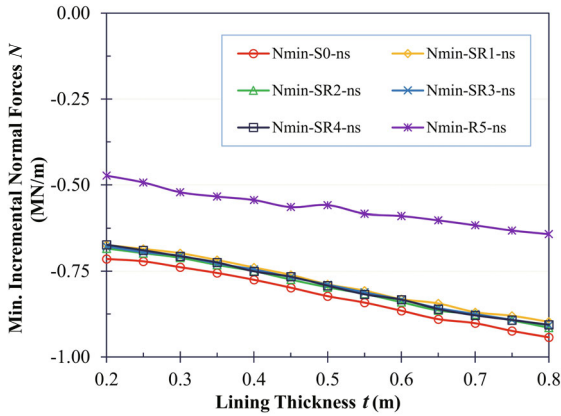


(d) Min. incremental bending moment for full-slip conditions

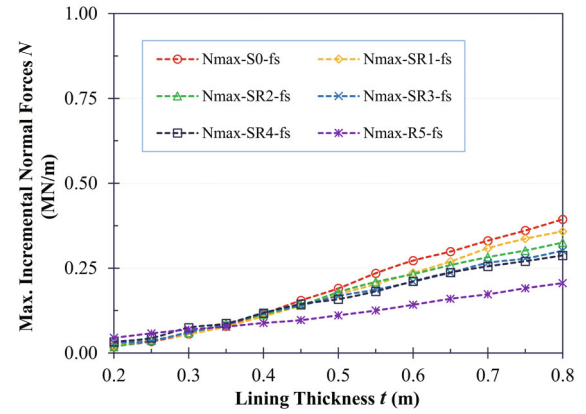
Fig. 13 Effect of lining thickness on the incremental bending moments of shaped tunnel linings



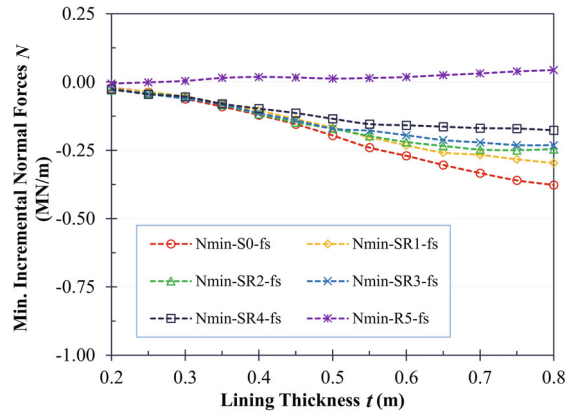
(a) Max. incremental normal forces for no-slip conditions



(c) Min. incremental normal forces for no-slip conditions



(b) Max. incremental normal forces for full-slip conditions



(d) Min. incremental normal forces for full-slip conditions

Fig. 14 Effect of lining thickness on the incremental normal forces of the shaped tunnel linings

SR4, the values of incremental normal forces of sub-rectangular tunnels decrease when their width/height ratio increases. Figure 14(d) also indicates that the compressive incremental normal forces are induced mostly in the rectangular tunnel lining, except for the thin linings of 0.2 m and 0.25 m, where small tensile incremental normal forces are observed at the side walls. This result supports the recommendation of the influence of lining rigidity on the previously mentioned normal forces transmission ability, given that tensile normal forces can be observed in flexible linings.

The research results, presented in Fig. 15, indicate a linear relationship between the Δ_{str}/Δ_{ff} ratio and the lining thickness for tunnels of different shapes. In general, the ratio (Δ_{str}/Δ_{ff}) decreases in the thicker lining. In no-slip analysis, the highest Δ_{str}/Δ_{ff} ratio value occurred in rectangular tunnels (Fig. 15(a)). This result implies that a rectangular tunnel lining experiences the largest displacements compared to other shapes, while the smallest displacements are usually observed in the sub-rectangular tunnel SR1. Nevertheless, in a full-slip analysis, the ratio Δ_{str}/Δ_{ff} in rectangular tunnels is

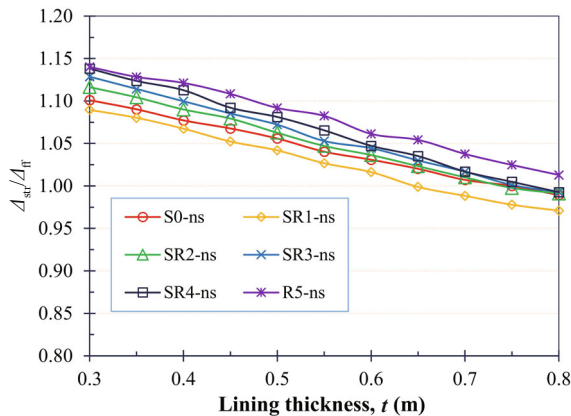
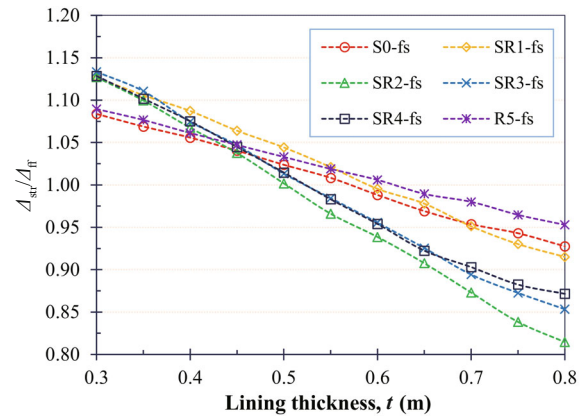

(a) Ratio Δ_{str}/Δ_{ff} in no-slip condition

(b) Ratio Δ_{str}/Δ_{ff} in full-slip condition

Fig. 15 Effect of lining thickness (t) on the relative ratio of displacements of lining and surrounding soil in considering different shaped tunnels

larger when the lining thickness is greater than 0.55 m (Fig. 15(b)). When the lining thickness is less than 0.45 m, the circular tunnel induces the smallest lining displacements. The same behavior is observed for the sub-rectangular tunnel SR2, which has a thicker lining.

5.4 Influence of the lining rigidity

The segmental lining is known as an efficient structure that performs well in seismic conditions. The presence of joints results in a flexural rigidity reduction of the segmental lining. In the present study, the influence of joints is considered by using a reduction factor, η , assigned to the bending rigidity (EJ) of the segmental tunnel lining:

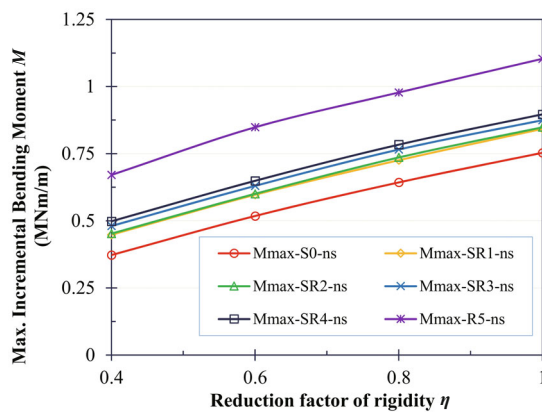
$$\eta = \frac{(EJ)_{eq}}{EJ} \quad (2)$$

where $(EJ)_{eq}$ is the segmental lining's flexural rigidity and EJ is the continuous lining's flexural rigidity (without joints). The value of $(EJ)_{eq}$ is determined by multiplying the original stiffness (EJ) of the continuous lining by the reduction factor (η) to consider the influence of segmental joints.

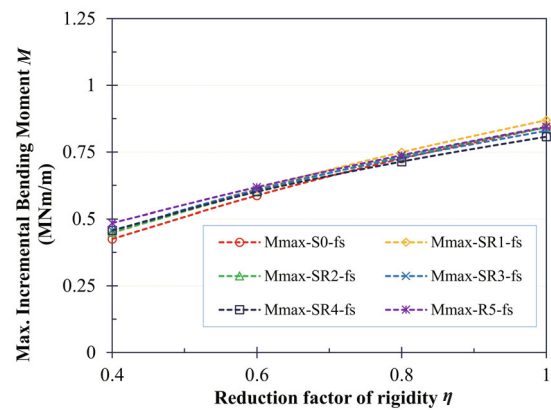
The reduction factor (η), usually falls in the range of 0.6 to 0.8 for circular tunnels (Koyama and Nishimura, 1998). Four η values, equal to 0.4, 0.6, 0.8, and 1, were

adopted in the present study to cover a wide range of tunnel shapes, i.e., sub-rectangular and rectangular.

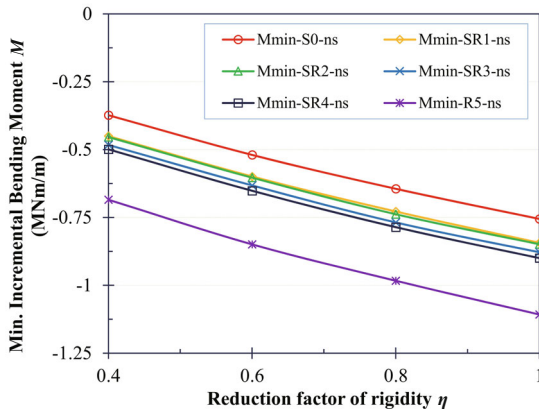
Figure 16 indicates that the reduction factor of lining rigidity (η) exerts a significant impact on the extreme incremental bending moments in the tunnel lining. It is noted that an increase in the lining rigidity reduction factor (η) also means a stiffer lining, and therefore the ground tends to be more resistant due to the presence of the lining. Hence, it is followed by an increase in the absolute extreme incremental bending moments for both the no-slip and full-slip analyses. The relationship between the extreme incremental bending moments and the reduction factor (η) is close to a linear function shape. It should be mentioned that when considering the change in the reduction factor of the lining's flexural rigidity, a larger influence of tunnel shape is seen by means of the no-slip analysis (Figs. 16(a) and 16(c)). Meanwhile, in most of the reduction factors (η) in full-slip analysis, the values of extreme incremental bending moments obtained for different tunnel cases are very close to one another (Figs. 16(b) and 16(d)). Furthermore, the tunnel shape has a significant effect on the stress redistribution induced in the soil surrounding the tunnel, particularly the tangential stress components, which usually reach their maximum values near the tunnel boundary (Panthi, 2006; Wael *et al.*, 2018). Nevertheless, because of the tangential tension loss along the tunnel periphery in the full slip analysis, the tangential stress effect induced in



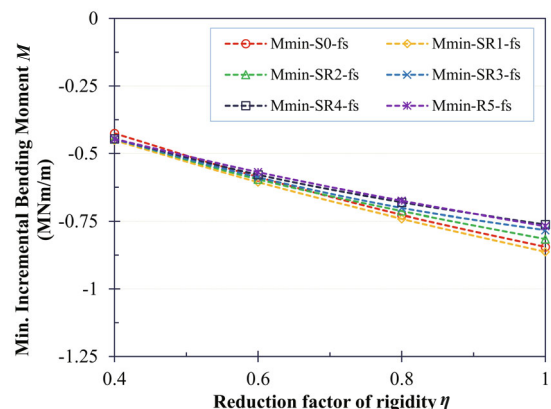
(a) Max. incremental bending moments for no-slip conditions



(b) Max. incremental bending moments for full-slip conditions



(c) Min. incremental bending moments for no-slip conditions



(d) Min. incremental bending moments for full-slip conditions

Fig. 16 Effect of the rigidity factor reduction (η) on the incremental bending moments of tunnel linings

the soil transmitted to the tunnel lining is reduced when compared to the one in the case of the no-slip analysis. The same findings are presented by Fang *et al.* (2023), who emphasized that when the ground-lining interface is imperfect, the stresses in the tunnel linings decrease due to the lack of efficiency in transmitting wave energy.

Therefore, an insignificant influence for different tunnel shapes could be expected with regard to the lining rigidity reduction factors (η) in the full-slip analysis. In contrast to the bending moments, Fig. 17 indicates an insignificant impact of the reduction factor (η) on the extreme incremental normal forces.

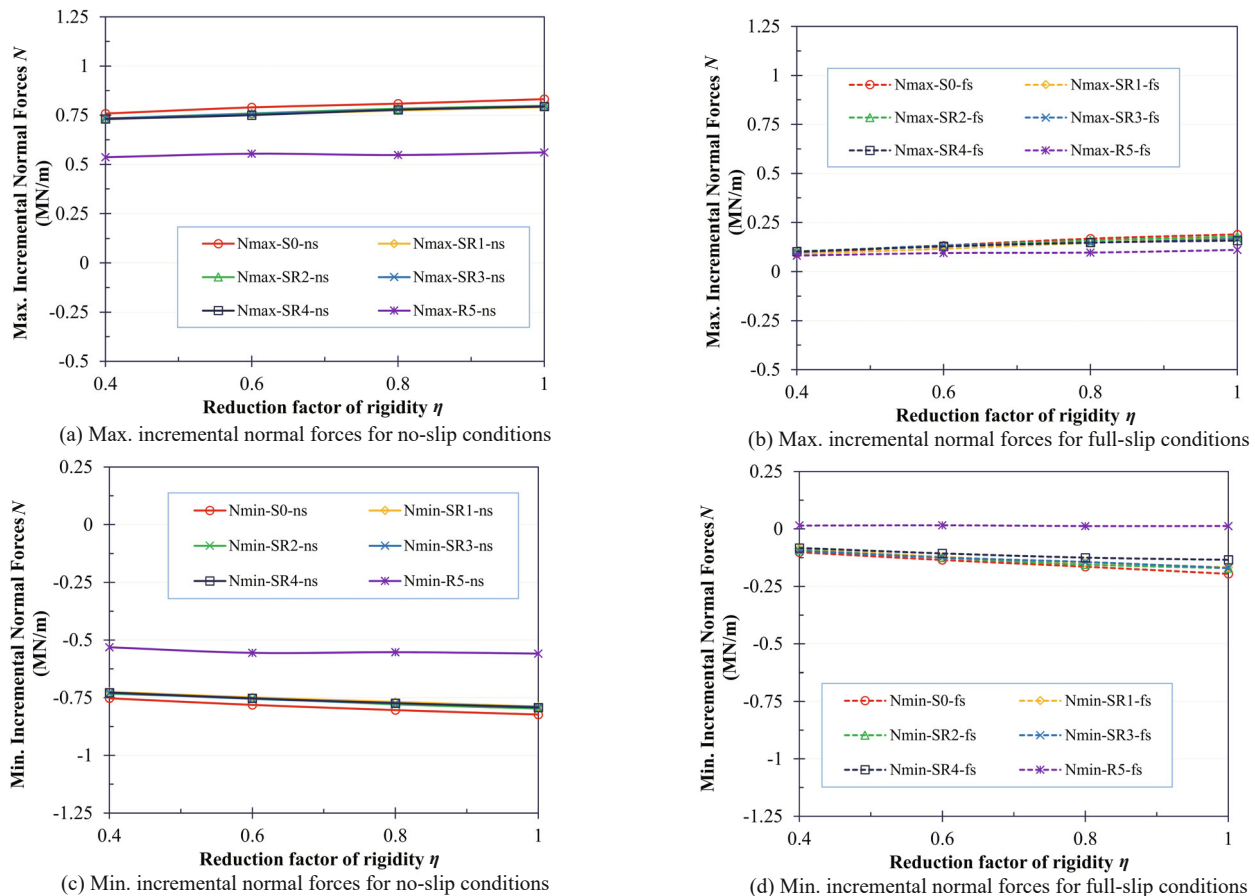


Fig. 17 Effect of the rigidity factor reduction (η) on the incremental normal forces of tunnel linings

6 Conclusions

In the present study, 2D numerical analyses were conducted to investigate the behavior of tunnels with different geometries, under quasi-static conditions by considering the influence of parameters such as soil-lining interaction, soil parameters, and lining thickness, as well as lining rigidity. Two cases of circular and rectangular tunnels and four sub-rectangular tunnel shapes that have a similar excavated cross-section area were proposed for the numerical analysis. The following comments can be drawn based on the results obtained:

(1) The tunnel shape and soil-lining interaction for the no-slip and full-slip conditions have a great impact on lining behavior under quasi-static conditions.

(2) The absolute extreme incremental bending moments for circular tunnels in the full-slip condition are greater than the corresponding ones for the no-slip condition. However, the soil-lining interaction influencing the absolute extreme incremental bending

moments for the sub-rectangular tunnels depends upon the ratio between the tunnel's width (B) and height (H_t). When the B/H_t ratio increases, the absolute extreme incremental bending moments for the no-slip condition tend to increase as well. Their values for the full-slip conditions are reduced and become even smaller than those obtained for the no-slip condition. For the particular case of rectangular tunnels, their values for the no-slip condition are greater than those corresponding to the full-slip analyses.

(3) Absolute extreme incremental normal forces induced for the no-slip condition are always greater than those computed for the full-slip condition. The greatest incremental normal forces are obtained for circular tunnels, while a rectangular tunnel induces the smallest incremental normal forces, and the values for sub-rectangular tunnels fall in the range in between. Moreover, incremental normal forces induced in the rectangular tunnel during a full-slip analysis are usually greater than zero, which indicates the impact

of compressive incremental normal forces in the tunnel lining.

(4) The maximum horizontal acceleration (a_H) influence on the extreme incremental bending moments induced in the circular tunnel and rectangular tunnel is different from the sub-rectangular tunnel for the no-slip analysis. The rectangular tunnels are the most sensitive structures, and the circular tunnels are less influenced by the change in a_H values, while the values for sub-rectangular tunnels fall into the range in between.

(5) Considering the soil Young's modulus variation and lining thickness, the absolute extreme incremental bending moments and normal forces in the sub-rectangular tunnels are similar.

(6) The ratio between the maximum displacements of the lining and the soil in the free zone (Δ_{str}/Δ_{fr}) increases with the higher soil Young's modulus and thinner lining.

(7) The bending lining rigidity has a remarkable influence on the extreme incremental bending moments in the tunnel lining. However, it causes an insignificant impact on the extreme incremental normal forces.

The numerical results presented in the present study present a preliminary understanding of the behavior of differently shaped tunnel structures under quasi-static loading conditions. Analyses using a real seismic wave will be considered in future research.

Acknowledgement

This study was supported by Vietnam Ministry of Education and Training under Grant No. B2022-MDA-06.

References

- Abate G, Grasso S and Massimino MR (2023), "Effect of Soil Heterogeneity on Seismic Tunnel Lining Forces," *Soil Dynamics and Earthquake Engineering*, **168**: 107849.
- Abate G, Massimino MR and Maugeri M (2015), "Numerical Modelling of Centrifuge Tests on Tunnel-Soil Systems," *Bulletin of Earthquake Engineering*, **13**: 1927–1951. <https://doi.org/10.1007/s10518-014-9703-0>
- Baziar MH, Moghadam MR, Choo YW and Kim DS (2016), "Tunnel Flexibility Effect on the Ground Surface Acceleration Response," *Earthquake Engineering and Engineering Vibration*, **15**(3): 457–476. <https://doi.org/10.1007/s11803-016-0336-y>
- Bobet A (2003), "Effect of Pore Water Pressure on Tunnel Support During Static and Seismic," *Tunnelling and Underground Space Technology*, **18**: 377–393.
- Chen G, Yu HT and Bobet A (2022), "Analytical Solution for Seismic Response of Deep Tunnels with Arbitrary Cross-Section Shape in Saturated Orthotropic Rock," *Rock Mechanics and Rock Engineering*, **55**(10): 5863–5878.
- Chen X, Zhang K and Wang W (2023), "Seismic Stability Analysis of Tunnel Faces in Heterogeneous and Anisotropic Soils Using Modified Pseudodynamic Method," *Sustainability*, **15**(14): 11083. <https://doi.org/10.3390/su151411083>
- Chi TN and Alexandr G (2020), "Hyperstatic Reaction Method for Calculations of Tunnels with Horseshoe-Shaped Cross-Section Under the Impact of Earthquakes," *Earthquake Engineering and Engineering Vibration*, **19**(1): 179–188. <https://doi.org/10.1007/s11803-020-0555-0>
- Cho MD, Tang A, Huang D and Zhang J (2021), "Large Scale Shaking Table Model Test and Analysis on Seismic Response of Utility Tunnel in Non-Homogeneous Soil," *Earthquake Engineering and Engineering Vibration*, **20**(2): 505–515. <https://doi.org/10.1007/s11803-021-2035-6>
- Choudhury D, Patil M, Ranjith PG and Zhao J (2019), "Dynamic Tunnel-Soil Interaction in Soft Soils Considering Site-Specific Seismic Ground Response," In: GM Latha, editors, *Frontiers in Geotechnical Engineering: Developments in Geotechnical Engineering*, Springer, Singapore, pp. 249–271. https://doi.org/10.1007/978-981-13-5871-5_12
- Di HG, Guo HJ, Zhou SH, Wang BL, He C and Zhang XH (2022), "An Analytical Model for Evaluating the Dynamic Response of a Tunnel Embedded in Layered Foundation Soil with Different Saturations," *Earthquake Engineering and Engineering Vibration*, **21**(3): 663–681. <https://doi.org/10.1007/s11803-022-2120-5>
- Do NA, Dias D and Oreste PP (2014), "2D Seismic Numerical Analysis of Segmental Tunnel Lining Behaviour," *Bulletin of the New Zealand Society for Earthquake Engineering*, **47**(3): 206–216.
- Do NA, Dias D, Oreste PP and Djeran-Maigre I (2015), "2D Numerical Investigation of Segmental Tunnel Lining Under Seismic Loading," *Soil Dynamics and Earthquake Engineering*, **72**: 66–76. <https://doi.org/10.1016/j.soildyn.2015.01.015>
- Do NA, Dias D, Zhang ZX, Huang X, Nguyen TT, Pham VV and Nait-Rabah O (2020), "Study on the Behavior of Squared and Sub-Rectangular Tunnels Using the Hyperstatic Reaction Method," *Transportation Geotechnics*, **22**: 100321. <https://doi.org/10.1016/j.trgeo.2020.100321>
- Fang XQ, Ma HW, Zhu CS, Ding QL, Zhu ZG and Han ZM (2023), "Imperfect Interface Model and Dynamic Interaction Mechanism Around Tunnels Under Seismic Waves: A Review," *Tunnelling and Underground Space Technology*, **137**: 105120.
- Feizi D, Asgari Marnani J, Alielahi H and Panji M (2022), "Seismic Ground Amplification Induced by Box-Shaped Tunnels," *Earthquake Engineering and Engineering Vibration*, **21**(3): 697–714.
- FHWA (2004), *Seismic Retrofitting Manual for Highway Structures: Part 2 - Retaining Structures, Slopes,*

Tunnels, Culverts and Roadways, Publication No. FHWA-HRT-05-067, U.S. Department of Transportation, Federal Highway Administration, Washington, D.C., USA.

Golshani A and Rezaeibadashiani MA (2020), “Numerical Study on Parameters Affecting Seismic Behavior of Cut and Cover Tunnel,” *Geotechnical and Geological Engineering*, **38**: 2039–2060. <https://doi.org/10.1007/s10706-019-01147-x>

González-Nicieza C, Álvarez-Vigil AE, Menéndez-Díaz A and González-Palacio C (2008), “Influence of the Depth and Shape of a Tunnel in the Application of the Convergence-Confinement Method,” *Tunnelling and Underground Space Technology*, **23**(1): 25–37. <https://doi.org/10.1016/j.tust.2006.12.001>

Hashash YMA, Hook JJ, Schmidt B and Yao JIC (2001), “Seismic Design and Analysis of Underground Structures,” *Tunnelling and Underground Space Technology*, **16**: 247–293. [https://doi.org/10.1016/S0886-7798\(01\)00051-7](https://doi.org/10.1016/S0886-7798(01)00051-7)

Hashash YMA, Park D and Yao JIC (2005), “Ovaling Deformations of Circular Tunnels Under Seismic Loading, an Update on Seismic Design and Analysis of Underground Structures,” *Tunnelling and Underground Space Technology*, **20**: 435–441.

Hua N, Tessari A and Khorasani NE (2022), “The Effect of Geologic Conditions on the Fire Behavior of Tunnels Considering Soil-Structure Interaction,” *Tunnelling and Underground Space Technology*, **122**: 104380.

Itasca Consulting Group (2016), *FLAC Fast Lagrangian Analysis of Continua, Version 5.0, User's Manual*, Available: <https://www.itascacg.com/>.

Kouretzis G, Sloan SW and Carter JP (2013), “Effect of Interface Friction on Tunnel Liner Internal Forces Due to Seismic S- and P-Wave Propagation,” *Soil Dynamics and Earthquake Engineering*, **46**: 41–51.

Koyama Y and Nishimura T (1998), “Design of Lining Segment of Shield Tunnel Using a Beam-Spring Model,” In: *Quarterly Report of RTRI (Railway Technical Research Institute)*, Japan, **39**(1): 23–27.

Lanzano G, Bilotta E, Russo G and Silvestri F (2015), “Experimental and Numerical Study on Circular Tunnels Under Seismic Loading,” *European Journal of Environmental and Civil Engineering*, **19**(5): 539–563. <https://doi.org/10.1080/19648189.2014.893211>

Liu JB, Wang DY and Bao X (2021), “Longitudinal Integral Response Deformation Method for the Seismic Analysis of a Tunnel Structure,” *Earthquake Engineering and Engineering Vibration*, **20**(4): 887–904. <https://doi.org/10.1007/s11803-021-2060-5>

Liu X, Ye YH, Liu Z and Huang DZ (2018), “Mechanical Behavior of Quasi-Rectangular Segmental Tunnel Linings: First Results from Full-Scale Ring Tests,” *Tunnelling and Underground Space Technology*, **71**: 440–454.

Lu SS, Xu H, Wang LG, Liu SD, Zhao DX and Nie W (2022), “Effect of Flexibility Ratio on Seismic Response of Rectangular Tunnels in Sand: Experimental and Numerical Investigation,” *Soil Dynamics and Earthquake Engineering*, **157**: 107256.

Möller SC and Vermeer PA (2008), “On Numerical Simulation of Tunnel Installation,” *Tunnelling and Underground Space Technology*, **23**(4): 461–475.

Naggar HE, Hinchberge SD, Hesham M and Naggar EI (2008), “Simplified Analysis of Seismic In-Plane Stresses in Composite and Jointed Tunnel Linings,” *Tunnelling and Underground Space Technology*, **28**: 1063–1077.

Newmark NM (1967), “Problems in Wave Propagation in Soil and Rocks,” In: *Proceedings of the International Symposium on Wave Propagation and Dynamic Properties of Earth Materials*, Albuquerque, NM: University of New Mexico Press, USA, pp. 7–26.

Nguyen DD, Park D, Shamsher S, Nguyen VQ and Lee TH (2019), “Seismic Vulnerability Assessment of Rectangular Cut-and-Cover Subway Tunnels,” *Tunnelling and Underground Space Technology*, **86**: 247–261.

Nguyen TT, Do NA, Karasev MA, Dang VK and Dias D (2020), “Tunnel Shape Influence on the Tunnel Lining Behavior,” *Proceedings of the Institution of Civil Engineers - Geotechnical Engineering*, **174**(4): 355–371. <https://doi.org/abs/10.1680/jgeen.20.00057>

Panthi KK (2006), “Analysis of Engineering Geological Uncertainties Related to Tunnelling in Himalayan Rock Mass Conditions,” *Doctoral Thesis*, Norwegian University of Science and Technology, Norway.

Penzien Z (2000), “Seismically Induced Racking of Tunnel Linings,” *Earthquake Engineering & Structural Dynamics*, **29**: 683–691. [https://doi.org/10.1002/\(SICI\)1096-9845\(200005\)29:5<683::AID-EQE932>3.0.CO;2-1](https://doi.org/10.1002/(SICI)1096-9845(200005)29:5<683::AID-EQE932>3.0.CO;2-1)

Pham VV, Do NA and Dias D (2021), “Sub-Rectangular Tunnels Behavior Under Seismic Loading,” *Applied Sciences*, **11**(21): 9909. <https://doi.org/10.3390/app11219909>

Pham VV, Do NA, Dias D, Nguyen CT and Dang VK (2023), “Sub-Rectangular Tunnels Behavior Under Static Loading,” *Transportation Infrastructure Geotechnology*, **10**(3): 488–503. <https://doi.org/10.1007/s40515-022-00230-w>

Pham VV, Do NA, Vo TH, Dias D, Nguyen CT and Do XH (2022), “Effect of soil Young's Modulus on Sub-rectangular Tunnels Behavior Under Quasi-Static Loadings,” *Journal of Mining and Earth Sciences*, **63**(3a): 10–21. DOI: 10.46326/JMES.2022.63(3a).02

Sandoval E and Bobet A (2020), “Seismic Response of Underground Structures Under Undrained Loading with Excess Pore Pressures Accumulation,” *Tunnelling and Underground Space Technology*, **99**: 103255.

- Sederat H, Kozak A, Hashash YMA, Shamsabadi A and Krimotat A (2009), "Contact Interface in Seismic Analysis of Circular Tunnels," *Tunnelling and Underground Space Technology*, **24**: 482–490.
- Shadabi S, Moghadam MR and Parvizi M (2022), "Effect of Geofoam as Cover Material in Cut and Cover Tunnels on the Seismic Response of Ground Surface", *Earthquake Engineering and Engineering Vibration*, **21**(1): 67–80. <https://doi.org/10.1007/s11803-022-2076-5>
- Sun QQ, Du DC and Dias D (2020), "An Improved Hyperstatic Reaction Method for Tunnels Under Seismic Loading," *Tunnelling and Underground Space Technology*, **108**: 103687. <https://doi.org/10.1016/j.tust.2020.103687>
- Swati S, Sowmiya C and Swapnil M (2024), "Numerical Analysis of Moving Train Induced Vibrations on Tunnel, Surrounding Ground and Structure," *Earthquake Engineering and Engineering Vibration*, **23**(1): 179–192. <https://doi.org/10.1007/s11803-024-2223-2>
- Tsinidis G, Pitilakis K and Madabhushi G (2016a), "On The Dynamic Response of Square Tunnels in Sand," *Engineering Structures*, **125**(15): 419–437.
- Tsinidis G, Pitilakis K and Trikalioti AD (2014), "Numerical Simulation of Round Robin Numerical Test on Tunnels Using a Simplified Kinematic Hardening Model," *Acta Geotech*, **9**(4): 641–659.
- Tsinidis G, Rovithis E, Pitilakis K and Chazelas JL (2016b), "Seismic Response of Box-Type Tunnels in Soft Soil: Experimental and Numerical Investigation," *Tunnelling and Underground Space Technology*, **59**: 199–214.
- Tsinidis G, Silva FD, Anastasopoulos I, Bilotta E, Bobet A, Hashash YM, He C, Kampas G, Knappett J, Madabhushi G, *et al.* (2020), "Seismic Behavior of Tunnels: From Experiments to Analysis," *Tunnelling and Underground Space Technology*, **99**: 103334.
- Vinod M and Khabbaz H (2019), "Comparison of Rectangular and Circular Bored Twin Tunnels in Weak Ground," *Underground Space*, **4**(4): 328–339.
- Wael RA, Mahrous AA and Hyung-Sik Y (2018), "Studying the Effect of Some Parameters on the Stability of Shallow Tunnels," *Journal of Sustainable Mining*, **17**(1): 20–33. <https://doi.org/10.1016/j.jsm.2018.02.001>
- Wang J, Liu HQ, Liu HB and Zou Y (2019), "Centrifuge Model Study on the Seismic Responses of Shield Tunnel," *Tunnelling and Underground Space Technology*, **92**: 103036.
- Wang JN (1993), *Seismic Design of Tunnels: A State-of-the-Art Approach*, Brinckerhoff Quade and Douglas Inc., New York, USA.
- Wen YM, Xin CL, Shen YS, Huang ZM and Gao B (2021), "The Seismic Response Mechanisms of Segmental Lining Structures Applied in Fault-Crossing Mountain Tunnel: The Numerical Investigation and Experimental Validation," *Soil Dynamics and Earthquake Engineering*, **151**: 107001.
- Wu Q, Ding XM, Zhang YL and Zhang YL (2023), "Numerical Analysis of Seismic Response of Rectangular Underground Structure in Coral Sand," *Underground Space*, **9**: 155–172. <https://doi.org/10.1016/j.undsp.2022.07.005>
- Wu H, Guo E, Wang J, Dai X and Dai C (2024), "Seismic Performance Evaluation of Water Supply Pipes Installed in a Full-Scale RC Frame Structure Based on a Shaking Table Test," *Earthquake Engineering and Engineering Vibration*, **23**(1): 163–178. <https://doi.org/10.1007/s11803-024-2232-1>
- Yang WB, Qian ZH, Tu JL, Zhou ZY, Yan QX, Fang Y and He C (2022), "Centrifuge Modelling of Ground-Borne Vibrations Induced by Railway Traffic in Underground Tunnels," *Earthquake Engineering and Engineering Vibration*, **21**(2): 517–528.
- Yoon JU, Han JW, Joo EJ and Shin JH (2014), "Effects of Tunnel Shapes in Structural and Hydraulic Interaction," *KSCE Journal of Civil Engineering*, **18**: 735–741. <https://doi.org/10.1007/s12205-014-1325-1>
- Yu ZH, Kulatilake PHSW and Jiang F (2020), "Effect of Tunnel Shape and Support System on Stability of a Tunnel in a Deep Coal Mine in China," *Geotechnical and Geological Engineering*, **30**: 383–394. <https://doi.org/10.1007/s10706-011-9475-0>
- Yue CH and Zheng YL (2019), "Shaking Table Test Study on Seismic Behavior of Underground Structure with Intermediate Columns Enhanced by Concrete-Filled Steel Tube (CFT)," *Soil Dynamics and Earthquake Engineering*, **127**: 105838. <https://doi.org/10.1016/j.soildyn.2019.105838>
- Zhang JL, Schlappal T, Yuan Y, Mang HA and Pichler B (2019), "The Influence of Interfacial Joints on the Structural Behavior of Segmental Tunnel Rings Subjected to Ground Pressure," *Tunnelling and Underground Space Technology*, **84**: 538–556.
- Zhang YJ, Huang HW, Zhang DM and Ayyub BM (2022), "Deformation Recoverability of Longitudinal Joints in Segmental Tunnel Linings: An Experimental Study," *Tunnelling and Underground Space Technology*, **124**: 104475. <https://doi.org/10.1016/j.tust.2022.104475>
- Zhang ZX, Zhu YT, Zhu YF, Huang X and Zhuang QW (2017), "Development and Application of a 1:1 Mechanical Test System for Special-Shaped Shield Lining with a Large Cross-Section," *Chinese Journal of Rock Mechanics and Engineering*, **12**(36): 2895–2905. (in Chinese)